Effect of strain rate on the formation of nanocrystallites in an Al-based amorphous alloy during nanoindentation

W. H. Jiang
Department of Nuclear Engineering and Radiological Sciences, University of Michigan, Ann Arbor, Michigan 48109

F. E. Pinkerton
General Motors R&D Center, 30500 Mound Road, Warren, Michigan 48090-9055

M. Atzmon[a)]
Department of Nuclear Engineering and Radiological Sciences, University of Michigan, Ann Arbor, Michigan 48109 and Department of Materials Science and Engineering, University of Michigan, Ann Arbor, Michigan 48109

(Received 21 October 2002; accepted 11 March 2003)

The effect of deformation by nanoindentation on nanocrystallization in amorphous $Al_{90}Fe_5Gd_5$ was investigated by transmission electron microscopy. Massive precipitation of nanocrystallites is observed within the indents. Under the quasistatic condition used, a temperature rise due to adiabatic heating is likely negligible, confirming that plastic deformation can induce crystallization without a heating effect. The nucleation of nanocrystallites is significantly affected by the strain rate. © *2003 American Institute of Physics.* [DOI: 10.1063/1.1571234]

I. INTRODUCTION

Al-rich amorphous alloys, containing a few percent transition metal (TM) and rare-earth (RE) metal, have generated recent interest because their strength is higher than that of conventional high-strength Al alloys.[1,2] Nanometer-scale crystalline particles can be formed within the amorphous matrix through partial crystallization at elevated temperature, leading to significant strength enhancement.[3–6] Thus, nanocrystalline/amorphous Al–TM–RE composites are most promising as key structural materials. Since amorphous alloys are metastable, crystallization at elevated temperature is a result of the atomic diffusivity being sufficiently high to allow formation of equilibrium crystalline phases.

Chen *et al.*[7] found that mechanical deformation of some Al-rich amorphous alloys at room temperature also led to the formation of nanocrystallites. They reported that 180° bending of amorphous $Al_{90}Fe_5Gd_5$, $Al_{90}Fe_5Ce_5$, and $Al_{87}Ni_{8.7}Y_{4.3}$ at room temperature induced the formation of Al-rich nanocrystallites at shear bands. He *et al.*[8] demonstrated that high-energy ball milling also produced nanocrystalline Al-rich particles in several Al-based amorphous alloys. Recently, Gao *et al.*[9] observed the precipitation of nanocrystalline Al within vein protrusions on tensile fracture surfaces and along crack propagation paths, as well as within shear bands resulting from bending. However, no conclusion has been reached as to the mechanism of crystallization within shear bands. Csontos and Shiflet[10] suggested a temperature rise to play a crucial role in mechanically induced crystallization. They observed, using analytical transmission electron microscopy, radial diffusion fields of Gd and Fe associated with nanocrystals in amorphous $Al_{90}Fe_5Gd_5$ bent at room temperature. They argued that these resulted from a significant temperature increase during deformation. Indeed, bending or high-energy ball milling do not lend themselves to control of the strain rate. Both may induce highly localized deformation in a short time. It is, therefore, difficult to rule out a temperature rise as a cause of the formation of the nanocrystallites during deformation by bending or ball milling.

Nanoindentation provides a convenient and controlled method for introducing localized mechanical deformation into a material at room temperature at a sufficiently low rate to prevent a substantial increase in local temperature. Moreover, varying deformation rates can be employed in order to help determine the mechanism of deformation-assisted nanocrystallization. In this paper, we present transmission electron microscopy (TEM) observations on impressions formed by nanoindentation in amorphous $Al_{90}Fe_5Gd_5$. Preparation of TEM samples in which the thin area contained indents presented a challenge in this work.

II. EXPERIMENTAL PROCEDURE

The material investigated in this study is amorphous $Al_{90}Fe_5Gd_5$ (nominal composition in at. %). A ribbon, 22 μm thick and 1 mm wide, was obtained by single-wheel melt spinning using a Cr-coated copper wheel at a tangential velocity of 40 m/s in an Ar atmosphere. X-ray and electron diffraction analyses were used to verify the amorphous structure of the as-spun ribbons. A JEOL 4000 EX TEM was employed, operating at 400 kV. The instrumental camera length was used for lattice-parameter determination from diffraction patterns. Indentation experiments were performed using a Nanoinstruments Nanoindenter II with a diamond Berkovich indenter. The wheel side of the ribbon, to be used as the indenting surface, was polished with a single-side jet thinner. A solution of 25% nitric acid and 75% methanol at 243 K was used at a voltage of 90 V. The procedure is simi-

[a)]Electronic mail: atzmon@umich.edu

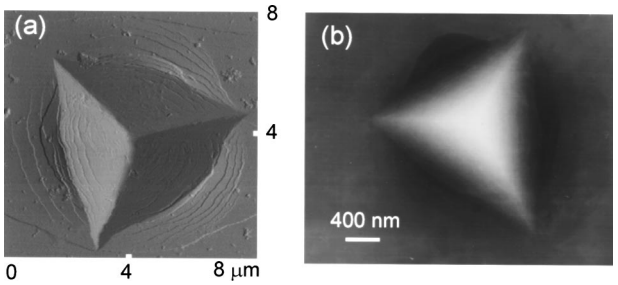

FIG. 1. Images of indented impressions formed at a loading rate of 100 nm/s. (a) AFM illumination mode image and (b) TEM bright-field image.

lar to that used to prepare TEM foils except that it was applied for a short duration without perforating the sample.

Numerous indents were made on each of multiple samples so that at least the area around one indent was likely to be sufficiently thin for subsequent observation in TEM. The loading phase of indentation was carried out under strain control at loading rates of 100 and 10 nm/s. The maximum indentation depth (elastic plus plastic) was 1 μm. In an indentation experiment, the strain rate ($\dot{\varepsilon}$) can be expressed as follows:

$$\dot{\varepsilon} = (1/h)(dh/dt), \tag{1}$$

where h and t are displacement and time, respectively. In the present work, loading was performed at constant displacement rates (dh/dt). Consequently, the strain rate ($\dot{\varepsilon}$) is inversely proportional to the displacement (h). The ratio of strain rates in two experiments is equal to that of displacement rates. For example, the strain rate at half the maximum displacement was 0.2 and 0.02 s^{-1}, respectively, for the presently used loading rates.

After nanoindentation, samples were thinned electrolytically from the surface opposite the indentations, using the same conditions as for surface preparation, except that a perforation was formed in each sample. To observe the indentation shape, atomic force microscopy (AFM) observation was conducted using a Digital Instruments Nanoscope IIIa in contact mode.

We performed a set of observations aimed at ruling out an artifact due to atomic displacements by the electrons in the TEM. We observed no detectable change in the microstructure of deformed and undeformed areas at a magnification of 100 K for constant exposure to the electron beam for up to 30 min. All the results we report were obtained by avoiding placing the focused beam at one position for a prolonged time. Our observations were generally performed at a magnification not higher than 100 K for less than 5 min. Selected-area electron diffraction (SAED) patterns were obtained in 1 or 2 min.

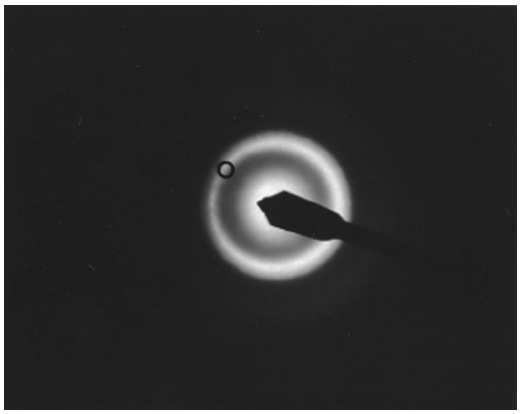

FIG. 2. Selected-area electron diffraction pattern in region near an impression bottom formed at a loading rate of 100 nm/s. The position and size of the objective aperture, used to establish the dark-field images, are indicated.

III. RESULTS AND DISCUSSION

Figure 1 shows typical AFM and TEM bright-field images of indented impressions. Discontinuous circular shear bands are observed within the impression. Similar features were also observed at a deformation rate of 10 nm/s, both being similar to those reported by Kim *et al.*[11] With increasing loading rate, for a fixed total strain, the number of shear band increases slightly, with a corresponding decrease in strain per shear band. These observations are discussed in Ref. 12.

Electron diffraction analysis was performed on indents that were perforated by electrolytic thinning. Only the regions near the bottom of the intents were sufficiently thin to yield visible electron diffraction patterns. The indents produced at deformation rates of both 100 and 10 nm/s possess similar diffraction patterns, four sharp rings plus diffuse rings originating from the amorphous matrix. Figure 2 shows such a typical diffraction pattern. The sharp diffraction rings correspond to the first four reflections of a face-centered-cubic phase with a lattice constant of 0.405 nm.

Using the {111} diffraction ring of the fcc phase, TEM dark-field images were obtained for the indents formed at 100 and 10 nm/s, respectively, as shown in Fig. 3. They reveal massive precipitation of nanocrystallites. Similar images were obtained when using other positions of the diffrac-

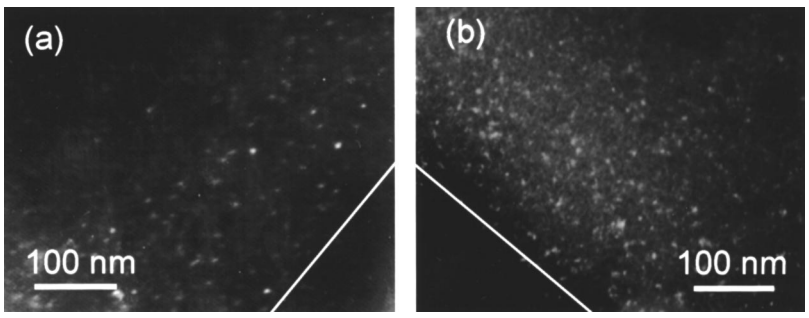

FIG. 3. TEM dark-field images established with the {111} ring of fcc phase (Fig. 2) in the indents formed at loading rates of (a) 100 nm/s and (b) 10 nm/s, respectively. Lines indicate edge of perforation.

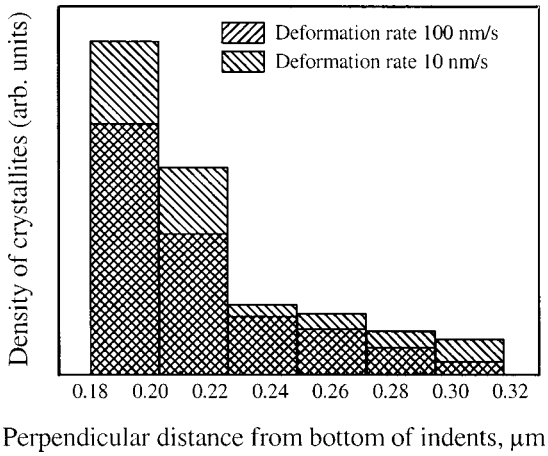

FIG. 4. Distribution of nanocrystallites within the indents.

tion ring, indicating isotropy of the crystallite orientation. The average diameters of the nanocrystallites formed at rates of 100 and 10 nm/s are 6.4 and 3.8 nm, respectively. Each value represents an average of approximately 60 nanocrystallites. The position-dependent average density of nanocrystallites is displayed in Fig. 4 for both strain rates. The absolute value of the density is difficult to determine because only a small fraction of the crystallites are imaged. The local sample thickness was determined based on the known indent shape. For both 100 and 10 nm/s, the nearer the bottom of the indents, the higher the densities of the nanocrystallites. This is a result of the fact that the bottom of the indent has experienced the greatest strain. The density at 10 nm/s is higher than that at 100 nm/s. These results demonstrate that the deformation rate has a significant influence on the nanocrystallization it induces.

It is highly unlikely that the nanocrystallites we observe form due to artifacts associated with TEM sample preparation. Samples that were cold-rolled in small steps, and then examined by x-ray diffraction, were observed to undergo partial crystallization. The use of jet thinning at subambient temperatures is unlikely to lead to temperatures above the crystallization temperature [220 °C (Ref. 8)]. Furthermore, samples that were not deformed, or even samples containing shear bands formed under tension,[13] did not contain nanocrystallites.

The structure and morphology of the nanocrystallites formed during nanoindentation appear to be the same as those in samples of the same alloy subjected to bending[7] and ball milling.[8] The lattice constant we observe, 0.405 nm, is close to that of pure Al, 0.404 14 nm.[14] Chen *et al.*[7] reported the lattice constant of fcc nanocrystallites in amorphous $Al_{90}Fe_5Gd_5$ bent at room temperature to be 0.4 nm, and suggested that they were essentially pure Al. Csontos and Shiflet[10] reported an approximate nanocrystallite composition of 95 at. % Al, 2 at. % Fe, and 2 at. % Gd. The lattice parameter we observe is in agreement with both results. As described above, nanocrystallization was suggested in Ref. 10 to result from a local temperature spike at shear bands. Also, Wright *et al.*[15] predicted a temperature increase as high as 280 K at fracture surfaces in amorphous Pd–Ni–P alloys. In fact, Gao *et al.*[9] observed melting, resulting from local adiabatic heating, at the fracture surface of a tensile sample. In the following discussion, we argue that, while a significant local temperature rise is possible under fracture conditions, no such rise, let alone any significant thermal diffusion length below the liquids temperature, is expected under low-rate nanoindentation. Chen *et al.*[7] estimated the local temperature increase at shear bands during bending to be as high as 2500 K. However, they also estimated that the heat generated was dissipated by conduction on a nanosecond timescale.[7,8] Since there is no driving force for crystallization above the melting point, this high cooling rate is expected to prevent crystallization. Kim *et al.*[11] estimated a temperature rise of 0.05 K in a bulk Zr-based amorphous alloy during nanoindentation at a rate similar to that used in the present study. We suggest that the formation of the nanocrystallites in amorphous $Al_{90}Fe_5Gd_5$ during nanoindentation results exclusively from mechanically produced defects. During the formation of shear bands, excess free volume is created. It assists atomic diffusion[16] similar to vacancies in crystalline solids. Such deformation-assisted diffusion toward thermodynamic equilibrium has been observed in amorphous and crystalline solids.[17–19]

Ye and Lu[20] found that the first crystallization temperature, at which fcc Al precipitated in amorphous $Al_{89}La_6Ni_5$, was lowered by hydrostatic pressure. They convincingly argued that this effect is due to an increased driving force for crystallization. They also extrapolated their results and predicted crystallization at room temperature under a pressure of about 2.5 GPa. We estimate the maximum hydrostatic stress in our experiments to be about 3.5 GPa. While it is uncertain whether the data of Ye and Lu can be extrapolated over a wide temperature range, their results indicate a potentially significant contribution to the driving force by the hydrostatic stress. Such a contribution would affect both the nucleation and growth of the nanocrystallites.

Our results indicate that a possible thermodynamic effect of the hydrostatic pressure is not dominant. The additional driving force due to the hydrostatic stress is the same at both strain rates, since the strain-rate sensitivity at room temperature is negligible.[21] Thus, if the thermodynamic effect were dominant, the sample deformed at a high rate (short time) would correspond to an early stage in the evolution of the sample deformed at a low rate (longer time). However, the crystallite size in the high-rate sample is greater. Thus, the rate effect is predominantly kinetic in origin.

In our observations, nanocrystallization is significantly affected by the deformation rate. At a high deformation rate, 100 nm/s, the nanocrystallites have a higher average diameter and lower density than at the lower deformation rate, 10 nm/s. Below, we suggest an interpretation of the higher nucleation rate at low strain rate, based on a kinetic argument. The difference in crystallite size can be attributed to the crystallite density: we estimate the average distance between crystallites at the bottom of the indent to be of the order of the crystallite size. This indicates that the diffusion fields of individual crystallites overlap. Therefore, the smaller crystallite size at 10 nm/s is a direct result of the higher density of nuclei. We note that the dependence of the

shear-band geometry on the loading rate[12] further strengthens this argument; a larger crystallite size is observed at the higher rate despite the smaller strain per shear band.

In order to evaluate the defect reactions that affect diffusion enhancement in a shear band, we consider a simple model of the kind often used to describe defect evolution in irradiated materials.[22] We will assume that during deformation, defects are generated at a rate K_o, which is proportional to the overall strain rate. For unimolecular defect annihilation kinetics, the annihilation rate is given by $k_1 c(t)$, where k_1 is a constant and $c(t)$ the instantaneous defect concentration. A steady state will be assumed. Since the observed variation of the number of shear bands with loading rate is weak, about a factor of 2 increase for an increase in loading rate by a factor of 100,[12] we first neglect it and subsequently consider its effect. We obtain

$$dc/dt = K_o - k_1 c(t). \tag{2}$$

When $k_1 t \gg 1$, one can assume steady state, with $c_{ss} = K_o/k_1$. It is now assumed that the effective diffusion coefficient is given by $D_{eff} = D_o c_{ss}$, where D_o is a constant. Since the nucleation rate is proportional to the effective diffusion coefficient,[23] the total number of nuclei, N_n, satisfies $N_n \propto N_s \int_0^{t_0} D_{eff} dt = N_s D_o c_{ss} t_o$ where t_o is the deformation time and N_s is the total area of shear bands in a sample. For a given maximum indentation depth, $t_o \propto 1/K_o$. Therefore, N_n is independent of K_o. The effect of the slight increase in N_s with increasing macroscopic strain rate,[12] is offset by the corresponding decrease in strain rate per shear band. For bimolecular defect annihilation kinetics, i.e., when the annihilation rate is given by $k_2 c(t)^2$, where k_2 is a constant, $c_{ss} = (K_o/k_2)^{1/2}$, and one obtains

$$N_n \propto N_s \int_0^{t_0} D_{eff} dt = N_s D_o c_{ss} t_o \propto N_s K_o^{-1/2}. \tag{3}$$

Thus, an increase in strain rate is predicted to decrease N_n. The physical origin of this result is that a higher fraction of the defects is annihilated if the same number of defects is generated at a high rate for a short time. For these kinetics, the small increase in N_s with increasing loading rate (about a factor of 2 for a 100-fold increase in strain rate, or roughly 1.4 for a tenfold increase in strain rate[12]), and the corresponding decrease in strain rate per shear band will diminish the variation of N_n with K_o in Eq. (3), but not reverse the trend. Equation (3), modified by the effect of increasing N_s with increasing loading rate, predicts N_n at 100 nm/s to be about half the value at 10 nm/s, as compared with about 0.75 in our experiment (see Fig. 4). Our data are not sufficient to allow a more detailed evaluation of this model. Further information about the variation of N_s and shear-band width with strain rate would be needed. However, the observed decrease in density of nuclei with strain rate tentatively suggests that defect annihilation kinetics are of order higher than first.

IV. CONCLUSIONS

Nanoindentation is observed to cause the formation of nanocrystallites in amorphous $Al_{90}Fe_5Gd_5$. Under such a quasistatic condition, a temperature rise due to adiabatic heating is likely negligible. Therefore, the observed diffusion at room temperature over distances of several nanometers is likely to be a result of nonequilibrium defect production. The observed dependence of the density of nuclei on the strain rate is tentatively suggested to reflect defect annihilation kinetics of order higher than first. Because of impingement of diffusion fields, a high density of nuclei leads to a smaller crystallite size. A potential thermodynamic effect of the hydrostatic stress is not dominant.

ACKNOWLEDGMENTS

The authors acknowledge useful discussions with Professor F. Spaepen (Harvard University). The electron microscopy and nanoindentation work was performed at the Electron Microbeam Analysis Laboratory at the University of Michigan. This work was funded by the U.S. National Science Foundation, Grant No. DMR-9902435.

[1] G. J. Shiflet, Y. He, and S. J. Poon, Scr. Metall. **22**, 1661 (1988).
[2] Y. He, G. J. Shiflet, and S. J. Poon, Scr. Metall. **22**, 1813 (1988).
[3] T. Kulik, J. Non-Cryst. Solids **287**, 145 (2001).
[4] H. Chen, Y. He, G. J. Shiflet, and S. J. Poon, Scr. Metall. Mater. **25**, 1421 (1991).
[5] Y. H. Kim, G. S. Choi, I. G. Kim, and A. Inoue, Mater. Trans., JIM **37**, 1471 (1996).
[6] W. S. Sun and M. X. Quan, Mater. Lett. **27**, 101 (1996).
[7] H. Chen, Y. He, G. J. Shiflet, and S. J. Poon, Nature (London) **367**, 541 (1994).
[8] Y. He, G. J. Shiflet, and S. J. Poon, Acta Metall. Mater. **43**, 83 (1995).
[9] M. C. Gao, R. E. Hackenberg, and G. J. Shiflet, Mater. Trans., JIM **42**, 1741 (2001).
[10] A. A. Csontos and G. J. Shiflet, Nanostruct. Mater. **9**, 281 (1997).
[11] J. J. Kim, Y. Choi, S. Suresh, and A. S. Argon, Science **295**, 654 (2002).
[12] W. H. Jiang and M. Atzmon, J. Mater. Res. **18**, 755 (2003).
[13] W. H. Jiang and M. Atzmon (unpublished work).
[14] W. B. Pearson, *Handbook of Lattice Spacing and Structures of Metals and Alloys* (Pergamon, London, 1958).
[15] W. J. Wright, R. B. Schwarz, and W. D. Nix, Mater. Sci. Eng., A **319-321**, 229 (2001).
[16] H. S. Chen, in *Amorphous Metallic Alloys*, edited by F. E. Luborsky (Butterworths, London, 1983).
[17] J. Xu and M. Atzmon, Appl. Phys. Lett. **73**, 1805 (1998).
[18] G. Mazzone, A. Montone, and M. Vittori Antisari, Phys. Rev. Lett. **65**, 2019 (1990).
[19] J. Xu, G. S. Collins, L. S. J. Peng, and M. Atzmon, Acta Mater. **47**, 1241 (1999).
[20] F. Ye and K. Lu, Acta Mater. **47**, 2449 (1999).
[21] W. H. Jiang and M. Atzmon (unpublished work).
[22] B. Park, F. Spaepen, J. M. Poate, D. C. Jacobson, and F. Priolo, J. Appl. Phys. **68**, 4556 (1990).
[23] H. Biloni and W. J. Boettinger, in *Physical Metallurgy*, edited by R. W. Cahn and P. Haasen (Elsevier Science B. V., Amsterdam, The Netherlands, 1996).